Effect of Protonation on Peroxo−Copper Bonding: Spectroscopic and Electronic Structure Study of $[Cu_2((UN-O-)(OOH)]^{2+}$

David E. Root,[†] Mohammed Mahroof-Tahir,[‡] Kenneth D. Karlin,[‡] and Edward I. Solomon*,[†]

Departments of Chemistry, Stanford University, Stanford, California 94305, and The Johns Hopkins University, Baltimore, Maryland 21218

Received May 29, 1998

Spectroscopic studies of a μ-1,1-hydroperoxo-bridged copper dimer are combined with SCF-Xα-SW molecular orbital calculations to describe the vibrational and electronic structure of the hydroperoxo−copper complex and compare it to that of previously studied peroxo−copper species. Four vibrational modes of the Cu_2OOH unit in the resonance Raman and infrared spectra are assigned on the basis of isotope shifts: ν(O−O) = 892 cm^{-1}, ν_{as}(Cu−O) = 506 cm^{-1}, ν_s(Cu−O) = 322 cm^{-1}, and ν(O−H) = 3495 cm^{-1}. The 892 cm^{-1} O−O stretch of the μ-1,1-hydroperoxo-bridged copper dimer is 89 cm^{-1} higher than that of the unprotonated complex. Resonance Raman profiles of the 892 cm^{-1} O−O stretch are used to assign an electronic absorption band at 25 200 cm^{-1} (ϵ = 6700 M^{-1} cm^{-1}) to a hydroperoxide π*-to-Cu charge transfer (CT) transition. This band is ∼5000 cm^{-1} higher in energy than the corresponding transition in the unprotonated complex. The π*-to-Cu CT transition intensity defines the degree of hydroperoxide-to-copper charge donation, which is lower than in the unprotonated complex due to the increased electronegativity of the peroxide with protonation. The lower Cu−O covalency of this hydroperoxo−copper complex shows that the high O−O stretching frequency is not due to increased π*-to-Cu charge donation but rather reflects the direct effect of protonation on intra-peroxide bonding. Density functional calculations are used to describe changes in intra-peroxide and Cu−O bonding upon protonation of the peroxo−copper complex and to relate these changes to changes in reactivity.

Introduction

Biological and synthetic copper complexes are catalysts for many important biological and industrial oxidation and oxygenation reactions.[1−3] Peroxo−copper and hydroperoxo−copper intermediates are proposed or observed in many of these reactions. The dioxygen transport protein hemocyanin contains a binuclear copper site that reversibly binds dioxygen as peroxide.[2,4] The enzyme tyrosinase binds dioxygen in the same manner as hemocyanin and activates the bound peroxide for oxidation of phenols to catechols.[5] Other copper-containing monooxygenases include dopamine-β-monooxygenase and peptidylglycine α-amidating monooxygenase which have been proposed to react via hydroperoxo−copper intermediates.[6] Hydroperoxo−copper intermediates have also been proposed for the multicopper[7,8] and copper amine[6] oxidases as well as copper−zinc superoxide dismutase.[9,10] The spectroscopic and chemical properties of peroxo−copper and hydroperoxo−copper species have consequently been the focus of considerable interest, yet relatively few such complexes have been characterized. The observed peroxo−copper binding modes are shown in Figure 1. Crystal structures have been obtained for two peroxo-bridged copper dimers, $[\{Cu(TMPA)\}_2(O_2)](PF_6)_2$ (where TMPA = tris(2-pyridylmethyl)-amine), in which the peroxide bridges the two copper ions in a trans μ-1,2 geometry[11] (Figure 1A) and $[Cu(HB(3,5\text{-}i\text{Pr}_2\text{pz})_3)]_2(O_2)$ (where $HB(3,5\text{-}i\text{Pr}_2\text{pz})_3$ = hydrotris-(3,5-diisopropylpyrazolyl)borate anion) in which peroxide binds in a side-on μ-η^2:η^2 geometry[12,13] (Figure 1B). For a third peroxo−copper complex, $[Cu_2(XYL-O-)(OO)]^+$ (where XYL−O = 2,6-bis[[bis[2-(2-pyridyl)ethyl]amino]methyl]-*p*-cresolate), a Raman isotope study showed the peroxide to be bound end-on to one copper ion[14,15] (Figure 1C). Our laboratory has studied these three best-defined examples of peroxo−copper complexes using resonance Raman and absorption spectroscopy and electronic structure calculations.[15−20] The present study

[†] Stanford University.
[‡] The Johns Hopkins University.

(1) Fox, S.; Karlin, K. D. In *Active Oxygen in Biochemistry*; Valentine, J. S., Foote, C. S., Greenberg, A., Liebman, J. F., Eds.; Blackie Academic & Professional: Glasgow, Scotland, 1995; pp 188−231.
(2) Solomon, E. I.; Baldwin, M. J.; Lowery, M. D. *Chem. Rev.* **1992**, *92*, 521−542.
(3) Kitajima, N.; Moro-oka, Y. *Chem. Rev.* **1994**, *94*, 737−757.
(4) Magnus, K. A.; Hazes, B.; Ton-That, H.; Bonaventura, C.; Bonaventura, J.; Hol, W. G. J. *Proteins* **1994**, *19*, 302.
(5) Solomon, E. I.; Sundaram, U. M.; Machonkin, T. E. *Chem. Rev.* **1996**, *96*, 2563−2605.
(6) Klinman, J. P. *Chem. Rev.* **1996**, *96*, 2541−2561.
(7) Shin, W.; Sundaram, U. M.; Cole, J. L.; Zhang, H. H.; Hedman, B.; Hodgson, K. O.; Solomon, E. I. *J. Am. Chem. Soc.* **1996**, *118*, 3202−3215.
(8) Sundaram, U. M.; Zhang, H. H.; Hedman, B.; Hodgson, K. O.; Solomon, E. I. *J. Am. Chem. Soc.* **1997**, *119*, 12525−12540.
(9) Holm, R. H.; Kennepohl, P.; Solomon, E. I. *Chem. Rev.* **1996**, *96*, 2239−2314.
(10) Ellerby, L. M.; Cabelli, D. E.; Graden, J. A.; Valentine, J. S. *J. Am. Chem. Soc.* **1996**, *118*, 6556−6561.
(11) Tyeklár, Z.; Jacobson, R. R.; Wei, N.; Murthy, N. N.; Zubieta, J.; Karlin, K. D. *J. Am. Chem. Soc.* **1993**, *115*, 2677−2689.
(12) Kitajima, N.; Fujisawa, K.; Moro-oka, Y.; Toriumi, K. *J. Am. Chem. Soc.* **1989**, *111*, 8975−8976.
(13) Kitajima, N.; Fujisawa, K.; Fujimoto, C.; Moro-oka, Y.; Hashimoto, S.; Kitagawa, T.; Toriumi, K.; Tatsumi, K.; Nakamura, A. *J. Am. Chem. Soc.* **1992**, *114*, 1277−1291.
(14) Karlin, K. D.; Cruse, R. W.; Gultneh, Y.; Farooq, A.; Hayes, J. C.; Zubieta, J. *J. Am. Chem. Soc.* **1987**, *109*, 2668−2679.
(15) Pate, J. E.; Cruse, R. W.; Karlin, K. D.; Solomon, E. I. *J. Am. Chem. Soc.* **1987**, *109*, 2624−2630.
(16) Baldwin, M. J.; Ross, P. K.; Pate, J. E.; Tyeklar, Z.; Karlin, K. D.; Solomon, E. I. *J. Am. Chem. Soc.* **1991**, *113*, 8671−8679.

S0020-1669(98)00606-5 CCC: $15.00
Published on Web 08/27/1998

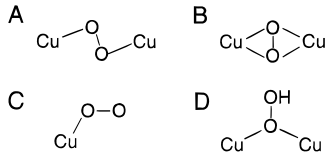

Figure 1. The four observed peroxo−copper binding geometries: (A) trans μ-1,2, $[\{Cu(TMPA)\}_2(O_2)]^{2+}$; (B) side-on μ-η^2:η^2, $[Cu(HB(3,5\text{-}i\text{Pr}_2\text{pz})_3)]_2(O_2)$; (C) end-on η^1, $[Cu_2(XYL-O-)(OO)]^+$; (D) μ-1,1-hydroperoxo, $[Cu_2(UN-O-)(OOH)]^{2+}$.

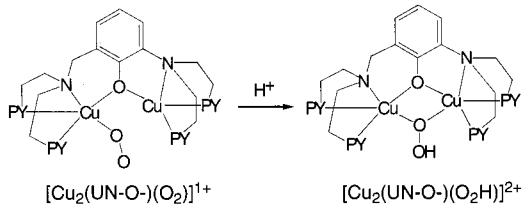

Figure 2. Protonation of the end-on complex $[Cu_2(UN-O-)(O_2)]^+$ (left), generating the μ-1,1-hydroperoxo-bridged dimer $[Cu_2(UN-O-)(OOH)]^{2+}$ (right).

extends this series by presenting spectroscopic and electronic structure characterization of the μ-1,1-hydroperoxo-bridged (Figure 1D) copper dimer $[Cu_2(UN-O-)(OOH)]^{2+}$ (Figure 2, right).[21]

Although an increasing number of transition metal hydroperoxide complexes have been synthesized, few of these complexes have been spectroscopically characterized. Only two hydroperoxo−copper complexes have been reported, the μ-1,1-hydroperoxo-bridged dimer $[Cu_2(UN-O-)(OOH)]^{2+}$ [21] (with several very close analogues, including $[Cu_2(XYL-O-)(OOH)]^{2+}$),[22] and a monomer, $Cu(HB(3\text{-}t\text{Bu-}5\text{-}i\text{Pr}_2\text{pz})_3)(OOH)$.[23] The $[Cu_2(UN-O-)(OOH)]^{2+}$ dimer can be generated by protonation of the corresponding peroxo complex (Figure 2). The structures of the μ-1,1-hydroperoxo-bridged dimers are inferred from the crystal structures of closely analogous species combined with EXAFS data. EXAFS studies of $[Cu_2(UN-O-)(OOH)]^{2+}$ and $[Cu_2(XYL-O-)(OOH)]^{2+}$ obtain Cu···Cu distances of 2.95(7) Å[21] and 3.04(6) Å,[22] respectively, considerably shorter than the 3.28(7) Å[21] and 3.31(4) Å[24] Cu···Cu distances in the corresponding unprotonated peroxo complexes. For the peroxo complex $[Cu_2(XYL-O-)(OO)]^+$, Raman isotope studies have shown that the peroxide is bound to only one of the two copper ions.[15] The 0.33 Å shortening of the Cu···Cu distance upon protonation strongly suggests a μ-1,1-bridging mode for the hydroperoxo complex. The most compelling evidence is provided by the crystal structure of $[Cu_2(XYL-O-)(OOAc)]^{2+}$, in which the acylperoxide bridges the two copper ions in a μ-1,1-geometry.[25] The electronic absorption spectrum of the μ-1,1-acylperoxo complex is strikingly similar to those of the $[Cu_2(UN-O-)(OOH)]^{2+}$ and $[Cu_2(XYL-O-)(OOH)]^{2+}$ complexes, indicating that these complexes have the same Cu−O binding geometry. An additional feature of the OOAc binding mode is that the carbon-bound peroxide oxygen of the acylperoxo group is slightly bent out of the plane formed by the copper-bound oxygen and the two copper ions. A cobalt dimer, $[(en)_2Co(NH_2,OOH)Co(en)_2](NO_3)_4$, has been found by crystallography to have the μ-1,1-hydroperoxide bridging geometry with the O−O vector bent out of the Co−O−Co plane.[26] It is interesting that the H_2OOH^+ ion also appears to have the same geometry for the R_2OOH unit where, in this case, $R = H^+$ rather than Cu or Co.[27]

In this paper, we report a vibrational and electronic spectroscopic study of the μ-1,1-hydroperoxo-bridged copper dimer $[Cu_2(UN-O-)(OOH)]^{2+}$. These results, combined with electronic structure calculations, are used to investigate the effects of protonation on intraperoxide and peroxo−copper bonding. A description of hydroperoxo−copper bonding is developed and compared to the bonding observed in previously studied peroxo−copper species. The significance of protonation for the activation and reduction of peroxide is discussed.

Experimental Section

The $[Cu^{II}_2(UN-O-)(OOH)](PF_6)_2$ solid samples and the dicopper(I) precursor $[Cu^{I}_2(UN-OH)](PF_6)_2$ for solution samples were prepared as reported previously.[21,28,29] Solutions of $[Cu_2(UN-O-)(OOH)]^{2+}$ were generated by oxygenation of $[Cu^{I}_2(UN-OH)](PF_6)_2$ in dichloromethane at −80 °C. UV/visible absorption spectra of $[Cu_2(UN-O-)(OOH)]^{2+}$ in dichloromethane solution were measured on a Perkin-Elmer 3840 spectrometer with a variable-temperature cryostat. Mull samples for infrared spectroscopy were prepared by grinding solid $[Cu_2(UN-O-)(OOH)](PF_6)_2$ in a precooled mortar under dry N_2 atmosphere and mulling with Nujol. Spectra were taken at room temperature with an IBM Bruker IR-98 FTIR spectrometer. The relative ν(OH) intensities for $[Cu_2(UN-O-)(OOH)](PF_6)_2$ and the $[Cu_2(UN-O-)(OH)](PF_6)_2$ decomposition product at 3495 and 3590 cm^{-1}, respectively, were used to monitor sample decomposition.

Resonance Raman spectra were obtained using a Princeton Instruments back-illuminated CCD detector on a Spex 1877 CP triple monochromator with 1200, 1800, and 2400 groove/mm holographic spectrograph gratings. The excitation was provided by Coherent I90K Kr^+ and CR18 Ar^+ CW ion lasers. A polarization scrambler was used between the sample and spectrometer. Spectral resolution was <2 cm^{-1}. Samples for solution Raman spectra were prepared by dissolving $[Cu_2(UN-OH)]$ in CH_2Cl_2 in an NMR tube and oxygenating at −78 °C. Solid Raman samples were prepared by dispersing $[Cu_2(UN-O-)(OOH)](PF_6)_2$ in KBr and K_2SO_4 in a dry ice cooled mortar under dry N_2. The sample tube was spun with an air-driven NMR spinner and cooled to ∼180 K by a N_2-flow system. A background spectrum of charcoal was subtracted to remove the Raman scattering of the quartz sample tube from the spectra. Integrated peak intensities for profiles were measured relative to the 700 cm^{-1} peak of CH_2Cl_2 for solution samples and relative to the 984 cm^{-1} peak of K_2SO_4 for solid samples. Raman spectra of solid samples could not be obtained with excitation wavelengths below 458 nm due to photodecomposition. Isotopic substitution of the OOH oxygens was accomplished by oxygenation of the complex with $^{18}O_2$ (Isotec, 99% labeled). The ^{18}OPh isotopic substitution was accomplished by reacting $[Cu^{I}(CH_3CN)_4]PF_6$ and the UN ligand in DMF with 99% $^{18}O_2$ to form $[Cu^{II}_2(UN-{}^{18}O-)(OH)](PF_6)_2$, which was then reduced by 1,1-diphenylhydrazine in diethyl ether to produce the $[Cu^{I}_2(UN-{}^{18}OH)](PF_6)_2$ precursor, from which $[Cu^{II}_2(UN-{}^{18}O-)(OOH)](PF_6)_2$ was formed by oxygenation at −78 °C.

(17) Baldwin, M. J.; Root, D. E.; Pate, J. E.; Fujisawa, K.; Kitajima, N.; Solomon, E. I. *J. Am. Chem. Soc.* **1992**, *114*, 10421−10431.
(18) Ross, P. K.; Solomon, E. I. *J. Am. Chem. Soc.* **1990**, *112*, 5871−5872.
(19) Ross, P. K.; Solomon, E. I. *J. Am. Chem. Soc.* **1991**, *113*, 3246−3259.
(20) Solomon, E. I.; Tuczek, F.; Root, D. E.; Brown, C. A. *Chem. Rev.* **1994**, *94*, 827−856.
(21) Mahroof-Tahir, M.; Murthy, N. N.; Karlin, K. D.; Blackburn, N. J.; Shaikh, S. N.; Zubieta, J. *Inorg. Chem.* **1992**, *31*, 3001−3003.
(22) Karlin, K. D.; Ghosh, P.; Cruse, R. W.; Farooq, A.; Gultneh, Y.; Jacobson, R. R.; Blackburn, N. J.; Strange, R. W.; Zubieta, J. *J. Am. Chem. Soc.* **1988**, *110*, 6769−6780.
(23) Fujisawa, K. Personal communication.
(24) Blackburn, N. J.; Strange, R. W.; Cruse, R. W.; Karlin, K. D. *J. Am. Chem. Soc.* **1987**, *109*, 1235−1237.
(25) Ghosh, P.; Tyeklár, Z.; Karlin, K. D.; Jacobson, R. R.; Zubieta, J. *J. Am. Chem. Soc.* **1987**, *109*, 6889−6891.
(26) Thewalt, U.; Marsh, R. *J. Am. Chem. Soc.* **1967**, *89*, 6364−6365.
(27) Christe, K. O.; Wilson, W. W.; Curtis, E. C. *Inorg. Chem.* **1979**, *18*, 2578−2586.
(28) Nasir, M. S.; Karlin, K. D.; McGowty, D.; Zubieta, J. *J. Am. Chem. Soc.* **1991**, *113*, 698−700.
(29) Mahroof-Tahir, M. Ph.D. Thesis, The Johns Hopkins University, 1992.

Normal-coordinate vibrational analysis was performed on a C_s symmetry model (Cu···Cu 2.95 Å, O−O 1.42 Å, Cu−O 1.93 Å, O−H 0.967 Å, OOH 99.5°). The normal-coordinate calculations used the Wilson **GF** matrix method as implemented in a modified Schachtschneider program.[30]

Electronic structure calculations using the 1982 QCPE version of the SCF-Xα-SW package were run on DEC 3100 and IBM 3BT-RS/6000 computers.[31−36] The exchange values, α, used in the atomic spheres are those of Schwarz.[37] The intersphere and outer-sphere α values were the valence-electron weighted average of the atomic α values. Norman sphere radii were used for all atoms except copper and oxygen. A copper sphere radius of 2.95 bohr was used rather than the Norman radius of ∼2.3 bohr. The 2.95 bohr Cu sphere radius has been found to better reproduce the ground-state g values in $CuCl_4^{2-}$ and plastocyanin.[38,39] Two sets of sphere radii were used for the peroxide oxygens to ensure that sphere radii did not bias comparisons of partitioned charges. In one set of calculations, Norman radii were used for the oxygen spheres, thus allowing the terminal oxygen sphere radius to contract upon addition of a proton. In a second set of calculations, both peroxide oxygen sphere radii were fixed at 1.74 bohr. The difference in partitioned charge on the oxygens between these two sets of calculations was negligible. A Watson sphere with a radius equal to that of the outer sphere and charge equal but opposite to that of the model was included for ionic models unless otherwise noted. Spin-restricted and spin-unrestricted calculations were performed with similar results. The criterion for convergence was a maximum relative change in atomic potentials for successive iterations of less than 10^{-4} Ry. The protonated models use the hydrogen peroxide parameters r(O−H) = 0.965 Å and θ(OOH) = 100°. The O_2^{2-} and HOO^- models use r(O−O) = 1.5 Å. The $(NH_3)_3CuOO$ and $[(NH_3)_3CuOOH]^+$ models have idealized square planar coordination geometry with r(Cu−N) = 2.03 Å. The 1.92 Å r(Cu−O) and 115° θ(CuOO) match those of the μ-1,1-hydroperoxo-bridged cobalt dimer $[(en)_2Co(NH_2,OOH)Co(en)_2](NO_3)_4$.[26] The 1.43 Å r(O−O) is the same as that in $[\{Cu(TMPA)\}_2(O_2)](PF_6)_2$ and 0.01 Å longer than that in the cobalt dimer.[11] The complete Cartesian coordinates are provided in the Supporting Information.

LCAO density functional calculations were performed using the 2.0.1 version of the Amsterdam Density Functional (ADF) programs developed by Baerends et al.[40] The Vosko−Wilk−Nusair local density approximation[41] for the exchange and correlation energy was used with the nonlocal gradient corrections of Becke and Perdew.[42,43] A triple-ζ Slater-type orbital (STO) basis set with single-ζ STO polarization function was used for all atoms. Filled shell orbitals were treated by the frozen-core approximation. Geometry optimizations were performed using the method of Ziegler et al.[44,45] provided in the ADF package.

(30) Schachtschneider, J. H. Technical Report No. 57-65; Shell Development Co.: Emeryville, CA, 1966.
(31) Johnson, K. H.; Norman, J. G., Jr.; Connolly, J. W. D. In *Computational Methods for Large Molecules and Localized States in Solids*; Herman, F., McLean, A. D., Nesbet, R. K., Eds.; Plenum: New York, 1973; pp 161−201.
(32) Slater, J. C. *The Self-Consistent Field for Molecules and Solids: Quantum Theory of Molecules and Solids*; McGraw-Hill: New York, 1974; Vol. 4.
(33) Connolly, J. W. D. In *Semiempirical Methods of Electronic Structure Calculation. Part A: Techniques*; Segal, G. A., Ed.; Plenum: New York, 1977.
(34) Cook, M. R. Ph.D. Thesis, Harvard University, 1981.
(35) Case, D. A. *Annu. Rev. Phys. Chem.* **1982**, *33*, 151−171.
(36) Cook, M.; Case, D. QCPE Program No. 465.
(37) Schwarz, K. *Phys. Rev. B* **1972**, *5*, 2466−2468.
(38) Gewirth, A. A.; Cohen, S. L.; Schugar, H. J.; Solomon, E. I. *Inorg. Chem.* **1987**, *26*, 1133−1146.
(39) Gewirth, A. A.; Solomon, E. I. *J. Am. Chem. Soc.* **1988**, *110*, 3811−3819.
(40) te Velde, G.; Baerends, E. J. *J. Comput. Phys.* **1992**, *99*, 84−98.
(41) Vosko, S. H.; Wilk, L.; Nusair, M. *Can. J. Phys.* **1980**, *58*, 1200−1211.
(42) Becke, A. D. *Phys. Rev. Rev. A* **1988**, *38*, 3098−3100.
(43) Perdew, J. P. *Phys. Rev. B* **1986**, *33*, 8800−8802.
(44) Verluis, L. Ph.D. Thesis, University of Calgary, 1989.
(45) Fan, L.; Ziegler, T. *J. Chem. Phys.* **1991**, *95*, 7401.

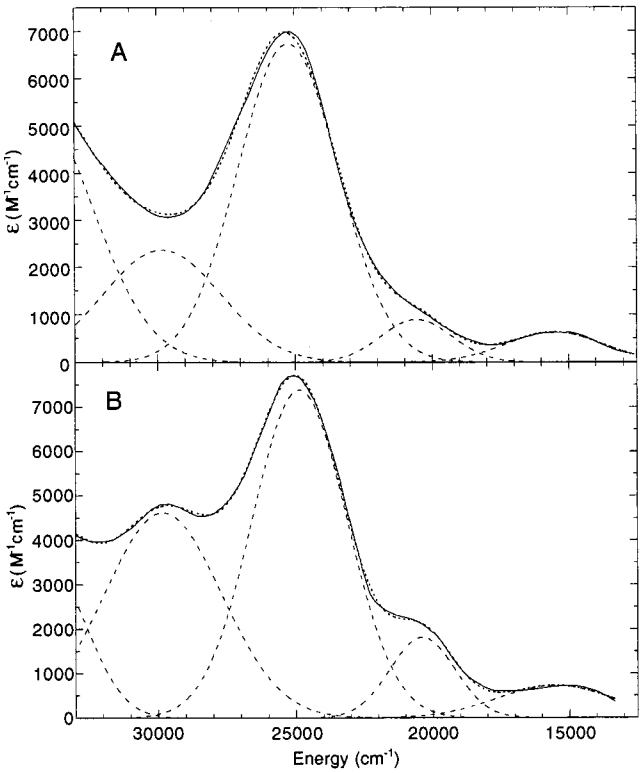

Figure 3. Absorption spectra of (A) $[Cu_2(UN-O-)(OOH)]^{2+}$ and (B) $[Cu_2\{(DMP)_4N6OH\}(OOH)]^{2+}$ in CH_2Cl_2 solution at −80 °C with Gaussian fits. Figure 3B is adapted from ref 46.

Results

Electronic Absorption Spectra. The absorption spectrum of $[Cu_2(UN-O-)(OOH)]^{2+}$ in dichloromethane at ∼200 K is shown in Figure 3A. The charge-transfer absorption spectrum of $[Cu_2(UN-O-)(OOH)]^{2+}$ exhibits a broad intense absorption feature at 25 200 cm^{-1} (ϵ = 7000 cm^{-1}) with a shoulder at ∼21 000 cm^{-1} and a band at 15 500 cm^{-1} (ϵ = 660 cm^{-1}). Sorrell has synthesized a series of analogues of the $[Cu_2(UN-O-)(OOH)]^{2+}$ complex in which pyrazolyl ligands replace two or four of the pyridyl ligands and several positions on the pyrazole or phenolate rings have either hydrogen or methyl groups.[46] These complexes all exhibit dichloromethane solution absorption spectra similar to that of the $[Cu_2(UN-O-)(OOH)]^{2+}$ complex but with small variations in band positions and intensities which permit better resolution of the absorption bands. Figure 3 shows Gaussian fits to the absorption spectra of $[Cu_2(UN-O-)(OOH)]^{2+}$ and Sorrell's $[Cu_2\{(DMP)_4N6OH\}(OOH)]^{2+}$ complex,[46] in which the pyridyl substituents of the UN−O ligand have been replaced by dimethylpyrazolyls and a methyl group replaces hydrogen in the para position of the phenolate. Table 1 gives the Gaussian fit parameters.

Raman and Infrared Spectra. Resonance Raman spectra of four isotopes of the hydroperoxo complex, $[Cu_2(UN-{}^{16}O-)({}^{16}O_2H)]^{2+}$, $[Cu_2(UN-{}^{16}O-)({}^{18}O_2H)]^{+}$, $[Cu_2(UN-{}^{18}O-)({}^{16}O_2H)]^{2+}$, and $[Cu_2(UN-{}^{18}O-)({}^{18}O_2H)]^{2+}$, in dichloromethane solution at ∼−80 °C with 406.7 nm (24 579 cm^{-1}) excitation are shown in Figure 4. The isotope-sensitive Raman peaks are listed in Table 2. Three Raman peaks at 892, 505, and 322 cm^{-1} shift with $^{18}O_2$ substitution of the hydroperoxide oxygens. Peaks at 1290, 870, 785, 740, and 643 cm^{-1} show the greatest sensitivity to isotopic substitution of the phenolate oxygen (Table

(46) Sorrell, T. N.; Vankai, V. A. *Inorg. Chem.* **1990**, *29*, 1687−1692.

Table 1. Gaussian Fit Parameters for −80 °C Solution Absorption Spectra[a]

	$[Cu_2(UN-O-)(O_2H)]^{2+}$			$[Cu_2\{(DMP_4)N6OH\}(O_2H)]^{2+}$		
	energy	intens	hwhm	energy	intens	hwhm
band 1	29 830[b]	2370	2500[c]	29 830	4610	2500[c]
band 2	25 240	6680	2150	24 860	7390	2030
band 3	20 580	890	1530	20 400	1810	1400
band 4	15 530	630	2070	15 540	730	2500[c]
band 5[d]	34 500	5540	2490	33 950	3360	1600

[a] Energy and hwhm are in cm^{-1}; intensity is in M^{-1} cm^{-1}. [b] Added to account for intensity tail from higher energy bands. [c] Fixed at energy of band 1 from $[Cu_2\{(DMP_4)N6OH\}(OOH)]^{2+}$. [d] Limited to an hwhm of 2500 cm^{-1}.

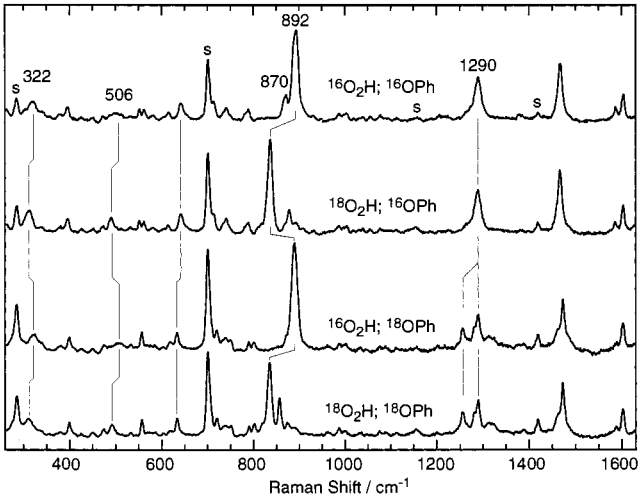

Figure 4. Resonance Raman spectra of four isotopes of $[Cu_2(UN-O-)(OOH)]^{2+}$ in CH_2Cl_2 solution at −80 °C using an excitation wavelength of 407 nm. Solvent bands are marked with an "s".

Table 2. Isotope-Sensitive Vibrational Frequencies of $[Cu_2(UN-O-)(OOH)]^{2+}$ in Wavenumbers (cm^{-1})

nat abund	$\Delta[^{18}O(Ph)]$	$\Delta[^{18}O_2(H)]$	$\Delta[^{18}O_2(H);^{18}O(Ph)]$
3495.0		−10.8	
892	−3	−55	−57
870	n.o.	+8	−13
506	∼−1	−15	−15
322	0	−10	−10
1290	+2, −33	0	+2, −33
785	+5, +20	0	+5, +20
740	−5, +10	0	−5, +10
643	−9	0	−9
563	−5, +5	0	−5, +5
396	+4	0	+4

2). The RR spectrum of solid $[Cu_2(UN-O-)(OOH)](PF_6)_2$ (not shown) also exhibits the $[^{18}O_2H]$ isotope-sensitive peak at 892 cm^{-1}. The infrared spectrum of solid $[Cu_2(UN-O-)(OOH)](PF_6)_2$ has a peak at 3495 cm^{-1} that shifts to 3484 cm^{-1} with $^{18}O_2$ isotope substitution. No other $^{18}O_2$ isotope sensitive peaks were observed in the IR spectrum of $[Cu_2(UN-O-)(OOH)](PF_6)_2$ between 400 and 4000 cm^{-1}. The resonance Raman enhancement profile of the most intense peak at 892 cm^{-1} is shown in Figure 5 and demonstrates that this mode is strongly enhanced by the 25 200 cm^{-1} absorption band.

Analysis

$Cu_2(OOH)$ Vibrational Assignments. Four peaks in the RR and IR spectra of $[Cu_2(UN-O-)(OOH)]^{2+}$ shift with $^{18}O_2$ isotopic substitution of the hydroperoxo bridge (Figure 4). These peaks are assigned to vibrations of the Cu(OOH)Cu unit.

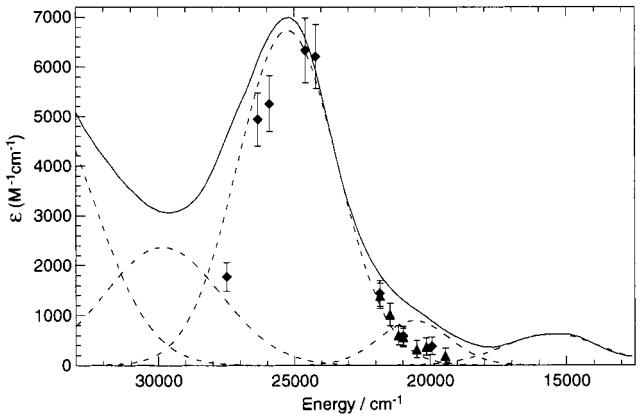

Figure 5. Resonance Raman excitation profiles of the 892 cm^{-1} O−O stretch of $[Cu_2(UN-O-)(OOH)](PF_6)_2$ solid (triangles) and solution in CH_2Cl_2 (diamonds) superimposed on the absorption spectrum with the Gaussian fit from Figure 3A.

The most intense peak in the RR spectrum at 892 cm^{-1} is assigned as the intra-peroxide stretch of the bridging hydroperoxide on the basis of its frequency and large isotope shift ($\Delta_{obs} = -55$ cm^{-1}, which corresponds to a shift of −52 cm^{-1} after correction for Fermi resonance; vide infra) with $^{18}O_2$ substitution. The RR peaks at 322 and 506 cm^{-1} are assigned as Cu−(O_2H)−Cu metal−ligand stretches on the basis of their frequencies and $^{18}O_2H$ isotope shifts.[47] A peak which appears at 3495 cm^{-1} in the infrared spectrum of solid $[Cu_2(UN-O-)(OOH)](PF_6)_2$ and shifts to 3484 cm^{-1} with the $^{18}O_2H$ isotope is assigned as the OO−H stretch of the hydroperoxide bridge.

The 892 cm^{-1} O−O stretching frequency of the hydroperoxo−copper complex is higher than that observed for any peroxo−copper complex and is in the upper range of intraperoxide stretching frequencies observed in peroxo-metal complexes (750−930 cm^{-1}).[48] This high-frequency implies a strong O−O bond, provided that the O−O stretching mode is not significantly coupled to other vibrational motions of the complex. Previously studied peroxo−copper complexes were found to have isolated O−O stretching modes on the basis of their $^{18}O_2$ isotope shifts and normal-coordinate analyses, including metal−ligand as well as O−O stretching frequencies.[15−17] For $[Cu_2(UN-O-)(O_2H)]^{2+}$, the large 52 cm^{-1} $^{18}O_2H$ isotope shift of the 892 cm^{-1} mode indicates that it is an isolated O−O stretch. For reasons described below, the $^{16}O-^{16}O$ and $^{18}O-^{18}O$ frequencies are best obtained from the $[^{16}O_2H;\ ^{18}OPh]$ and $[^{18}O_2H;\ ^{16}OPh]$ isotopes, which give a frequency isotope ratio of $\nu(^{16}O_2)/\nu(^{18}O_2) = 1.062$ ($\Delta\nu = 52$ cm^{-1} for $^{18}O-^{18}O$ of 837 cm^{-1}). This matches the frequency isotope ratio for a harmonic mode with oxygen motion only: $\nu(^{16}O_2)/\nu(^{18}O_2) = 1.061$ ($\Delta\nu = 50$ cm^{-1} for $^{18}O-^{18}O$ of 837 cm^{-1}).[49] The isotope shift would normally be reduced from the harmonic diatomic value if the 892 cm^{-1} mode involved motion of atoms other than oxygen. The $\nu(^{16}O_2)/\nu(^{18}O_2)$ ratios for $[Cu_2(XYL-O-)(O_2)]^+$, $[\{Cu(TMPA)\}_2(O_2)]^{2+}$, and $[Cu(HB(3,5\text{-}iPr_2pz)_3)]_2(O_2)$ are 1.071, 1.056, and 1.062, respectively, all near the oxygen-motion-only value, supporting similarly isolated O−O modes in these previously studied peroxo−copper complexes.[15−17] Vibrational isotope studies also find the O−O stretch to be a

(47) The ∼506 cm^{-1} peak overlaps the Raman scattering from the quartz sample tube and is obtained by subtraction of the quartz signal.

(48) Nakamoto, K. *Infrared Spectra of Inorganic and Coordination Compounds*, 3rd ed.; John Wiley & Sons: New York, 1978.

(49) Since the O−H frequency is much higher than the O−O frequency, it is reasonable to add the proton mass to the terminal oxygen mass for this simple diatomic model. The isotope ratio is not significantly affected: $\nu(^{16}O_2)/\nu(^{18}O_2) = 1.059$ ($\Delta\nu = 49$ cm^{-1}).

pure mode in gas phase and crystalline H_2O_2.[50,51] Thus, for all these peroxide species, the O−O frequency reflects the intrinsic stiffness of the O−O bond.

Isotope substitution of the phenolate oxygen provides a measure of involvement of Cu_2O_2 ring motions in the 892 cm^{-1} mode. The O−O stretch shifts slightly with ^{18}O substitution of the OPh bridging oxygen atom (−3 cm^{-1} for the [$^{16}O_2H$] isotopes and −2 cm^{-1} for the [$^{18}O_2H$] isotopes). This indicates that the 892 cm^{-1} mode involves some motion of the phenolate oxygen. The observed pattern of isotope shifts indicates that, for two of the four different isotopes, the 892 cm^{-1} peak is shifted by Fermi interactions with a phenolate-related mode at ∼878 cm^{-1}. The 870 cm^{-1} peak for the [$^{16}O_2H$;^{16}OPh] isotope disappears with ^{18}OPh isotope substitution (Figure 4), identifying it as a phenolate-related mode gaining intensity by Fermi resonance with the O−O stretch in the [$^{16}O_2H$;^{16}OPh] isotope. This peak appears shifted to 878 cm^{-1} for the [$^{18}O_2H$;^{16}OPh] isotope, in which Fermi resonance interaction is expected to be greatly diminished due to the −52 cm^{-1} shift in the O−O stretching frequency of the [$^{18}O_2H$] species. Thus, this ^{16}OPh mode has a frequency of ∼878 cm^{-1} in the absence of Fermi interaction with the O−O stretch. Using 458 nm excitation rather than 407 nm excitation, both the 870 and 892 cm^{-1} peaks lose intensity but the 870 cm^{-1} peak becomes much larger relative to the 892 cm^{-1} O−O stretching peak (see Supporting Information, p S5). This indicates that not all the 870 cm^{-1} intensity is derived from Fermi resonance; i.e., the phenolate mode gains some of its intensity from enhancement from a phenolate-to-Cu charge transfer (CT) transition. The O−O stretch in the [$^{18}O_2H$] isotopes appears to show Fermi interaction with this phenolate-related mode of the [$^{18}O_2H$;^{18}OPh] isotope but not of the [$^{18}O_2H$;^{16}OPh] isotope. Therefore, the O−O stretching frequencies in the absence of Fermi interaction may be obtained from the [$^{16}O_2H$;^{18}OPh] and [$^{18}O_2H$;^{16}OPh] isotopes. These frequencies are 889 cm^{-1} for $\nu(^{16}O-^{16}O)$ and 837 cm^{-1} for $\nu(^{18}O-^{18}O)$.

Normal-Coordinate Analysis for the Cu_2(OOH) Modes. A more detailed description of the Cu−(OOH)−Cu vibrational modes of $[Cu_2(UN-O-)(O_2H)]^{2+}$ is obtained from normal-coordinate analysis (NCA) on models consisting of the five atoms of the Cu−(OOH)−Cu unit. This NCA thus assumes no vibrational coupling of the Cu−(OOH)−Cu unit with the remainder of the molecule. The Cu−O stretches at 505 and 322 cm^{-1} shift by <2 cm^{-1} with ^{18}OPh isotope substitution and are thus not strongly coupled to motion of the bridging phenolate. The metal−ligand vibrations of the pyridine ligands, normally observed at <270 cm^{-1}, and the ammine nitrogen−metal stretch, expected in the 370−500 cm^{-1} range,[48] could potentially mix with one or both of the Cu−O stretches at 322 and 505 cm^{-1}; however, there is insufficient vibrational and structural information to warrant the inclusion of these ligands in the analysis. The Cu−(OOH)−Cu unit has nine vibrational degrees of freedom. To further simplify the calculations, internal coordinates allowing torsional motion were omitted, leaving a total of seven internal coordinates, of which five are symmetry-distinct.

A Urey−Bradley force field was used to fit the observed frequencies, facilitating comparison of the O−O and Cu−O stretching frequencies with those of previously studied peroxo complexes which were also analyzed using Urey−Bradley force fields.[15−17] Urey−Bradley nonbonded interaction force constants for the Cu−O−O and O−O−H internal coordinates were added to the five principal force constants. Since the CuOO and OOH bending modes were not observed for the hydroperoxo complex, the input frequencies for these modes were varied over the range observed for analogous molecules. The OOH bending frequencies for $H_3O_2^+$ and $HOONO_2$ are 1421 cm^{-1} [27] and 1397 cm^{-1}.[52] In gas-phase H_2O_2, the frequencies of the symmetric and asymmetric combinations of the OOH bends are 1393 and 1266 cm^{-1} respectively.[51]

Table 3. Normal-Coordinate Analysis of Cu_2OOH[a]

mode descripn	obsd freq $^{16}O_2$(H)	obsd freq $^{18}O_2$(H)	calcd freq $^{16}O_2$(H)	calcd freq $^{18}O_2$(H)	refined force constants internal coord	UB
O−H	3495	3484	3495	3484	F(O−H)	6.8
O−O−H	1300[b]		1300	1288	F(O−O)	3.7
O−O	880	837	887	839	F(Cu−O)	1.2
$(Cu-O)_{as}$	506	491	510	484	H(O−O−H)	0.8
$(Cu-O)_s$	322	312	325	311	H(Cu−O−O)	0.6
Cu−O−O	174[b]	170	176	168	K(O−O−H)	0.0[c]
Cu−O−O			166	160	K(Cu−O−O)	−0.2

[a] *F*, *H*, and *K* denote respectively the stretching, bending, and Urey−Bradley nonbonded force constants. Potential energy distributions of the O−O stretching and O−O−H bending modes are as follows. OO: 91% *F*(O−O) + 4% *H*(O−O−H) + 3% *F*(Cu−O). OOH: 96% *H*(O−O−H) + 4% *F*(O−O). [b] Estimate based on other complexes. [c] Fixed at zero.

Table 3 gives the input and calculated frequencies and force constants for a normal-coordinate calculation using the minimum values for the two Urey−Bradley (UB) force constants to give a reasonable fit to the frequencies. The potential energy distribution (PED) for the O−O stretching mode shows that it contains mostly the O−O internal coordinate combined with small contributions from the Cu−O symmetric stretch and the OOH bend internal coordinates. Varying the OOH or CuOO bending frequencies does not greatly increase the contributions of the Cu−O symmetric stretch and the OOH bend internal coordinates to the O−O stretching mode and thus does not strongly affect the calculated O−O force constant. The force field is underdetermined by the observed frequencies so that some force constants are interdependent. The O−O force constant was found to correlate strongly with the OOH UB nonbonded force constant. Good fits to the observed frequencies could be obtained using very large values of the OOH UB nonbonded force constant and resulted in lower values for the O−O force constant. Nevertheless, when all force constants including OOH UB are permitted to vary, this force field requires an O−O force constant of at least 3.3 mdyn/Å to obtain reasonable agreement with the observed O−O stretching frequency. This is higher than the Urey−Bradley (O−O) force constant obtained for previously characterized peroxo−copper complexes.[15−17] From this result, it is concluded that the high ν(O−O) does reflect a strong O−O bond and is not the result of mixing with other Cu−OOH−Cu modes. The Urey−Bradley NCA shown in Table 3 removes the OOH UB nonbonded force constant, giving an O−O force constant of 3.7 mdyn/Å. This value is more suitable than the 3.3 mdyn/Å lower limit for comparison with force constants from NCA of previously studied peroxo−copper complexes which used the minimum values for the UB force constants that provided a reasonable fit.[15−17] In addition to describing the O−O stretch as an isolated mode with a relatively high O−O force constant, the NCA allows assignment of the 506 and 322 cm^{-1} modes as the antisymmetric and symmetric Cu−O(OH)−Cu stretches, respectively.

(50) Arnau, J. L.; Giguère, P. A.; Abe, M.; Taylor, R. C. *Spectrochim. Acta* **1974**, *30A*, 777−796.
(51) Giguère, P. A.; Shrinivasan, T. K. *J. Raman Spectrosc.* **1974**, *2*, 125.
(52) Appleman, E. H.; Gosztola, D. J. *Inorg. Chem.* **1995**, *34*, 787−791.

Cu_2(OPh) Vibrational Assignments. The RR spectrum of $[Cu_2(UN-O-)(OOH)]^{2+}$ with 407 nm excitation (Figure 4) exhibits a number of other enhanced peaks in addition to the three peaks that shift with $^{18}O_2H$ substitution. The Cu_2O_2 ring can have a total of four stretching vibrations, the two Cu−O(OH)−Cu stretches at 322 and 506 cm^{-1} and two Cu−O(Ph)−Cu stretches. The peak at 643 cm^{-1} is assigned to be ν_s(Cu−O(Ph)−Cu) or ν_{as}(Cu−O(Ph)−Cu) due to its −9 cm^{-1} ^{18}OPh isotope shift. No other peaks observed in the this region of the Raman spectrum show comparably large shifts with ^{18}OPh isotope substitution. The 643 cm^{-1} peak does not shift with $^{18}O_2H$ isotope substitution, consistent with a lack of vibrational coupling between the two bridges. For a closely analogous hydroxo-bridged complex, $[Cu_2(XYL-O-)(OH)]^{2+}$, two of the Cu_2O_2 ring modes have been assigned as ν_{as}(Cu−O(Ph)−Cu) at 603 cm^{-1} (shifted by $\Delta = -11$ cm^{-1} for the ^{18}OPh isotope) and ν_s(Cu−O(H)−Cu) at 465 cm^{-1} (shifted by $\Delta = -12$ cm^{-1} for the ^{18}OH isotope).[53] These ν(Cu−O−Cu) peaks in $[Cu_2(XYL-O-)(OH)]^{2+}$ do not shift with isotope substitution of the second bridging group. Thus, strong mixing of the vibrations of the two bridges is not evident for either $[Cu_2(XYL-O-)(OH)]^{2+}$ or $[Cu_2(UN-O-)(OOH)]^{2+}$.

Phenolate−copper complexes have characteristic Raman bands at about 1280, 1480, and 1600 cm^{-1} which are resonance enhanced by phenolate-to-copper CT transitions.[54] These peaks are observed in the RR spectrum of $[Cu_2(UN-O-)(OOH)]^{2+}$ with 407 nm excitation at 1290, 1465, and 1600 cm^{-1} (Figure 4). The peaks at 1465, and 1600 cm^{-1} do not shift with ^{18}OPh isotope substitution and are assigned as ν(C−C) phenolate vibrations as in previous assignments.[54,55] The ν(C−O) of phenolate in aqueous solution is 1281 cm^{-1} and shifts to 1259 cm^{-1} ($\Delta = -22$ cm^{-1}) with ^{18}OPh isotope substitution.[56] The intense peak observed at 1290 cm^{-1} for $[Cu_2(UN-{}^{16}O-)(^{16}O_2H)]^{2+}$ is thus assigned as the phenolate ν(C−O). In the ^{18}OPh isotopes of $[Cu_2(UN-O-)(O_2H)]^{2+}$, two peaks are observed in this region at 1292 and 1257 cm^{-1}. The presence of these two intense peaks in the ^{18}OPh isotope may be attributed to a Fermi resonance of the shifted ν(C−O) vibration with another vibration in the same region. Due to the approximate 2:1 intensity ratio of the 1292 and 1257 cm^{-1} peaks, the 1290 cm^{-1} vibration has probably shifted to roughly a 2:1 weighted average of these frequencies (∼1280 cm^{-1}; $\Delta(^{18}\text{OPh}) \sim -10$ cm^{-1}). The frequencies of the phenolate bands are similar for the hydroxo-bridged analogue, $[Cu_2(XYL-O-)(OH)]^{2+}$, for which three Raman peaks are observed at 1310 ($\Delta(^{18}\text{OPh}) = -8$ cm^{-1}), 1473 and 1596 cm^{-1}, assigned to phenolate ν(C−O), and two phenolate ν(C−C) vibrations, respectively.[53,54]

Excited-State Assignments. The intense absorption feature at 25 200 cm^{-1} ($\epsilon_{max} = 7000$ M^{-1} cm^{-1}) in the charge-transfer absorption spectrum of $[Cu_2(UN-O-)(OOH)]^{2+}$ (Figure 3) is attributed to a hydroperoxo-to-Cu CT transition. The O−O stretch shows strong resonance Raman enhancement with a maximum around 25 000 cm^{-1}, supporting this assignment (Figure 5). For the unprotonated peroxo complex, $[Cu_2(UN-O-)(O_2)]^+$, the corresponding peroxo-to-Cu CT transition is at 19 900 cm^{-1} ($\epsilon_{max} = 6300$ M^{-1} cm^{-1}).[15] There are additional overlapping bands under the broad 25 200 cm^{-1} absorption band. Gaussian fitting of the absorption spectra of $[Cu_2(UN-O-)(OOH)]^{2+}$ and the analogous $[Cu_2\{(DMP)_4N6OH\}(OOH)]^{2+}$ complex shows there are at least three electronic transitions under this band (Figure 3) which are assigned as phenolate-to-copper CT and/or additional hydroperoxo-to-Cu CT transitions. The broad absorption feature at 15 500 cm^{-1} is typical for d−d transitions of a square pyramidal Cu(II) complex.

Peroxide and hydroperoxide have two donor orbitals, the degenerate π^* orbitals which are split by interaction with the metal ions and the proton. For previously studied peroxo−copper complexes, two peroxo-to-Cu CT transitions were observed, one for each of the two π^* orbitals of peroxide. The π^*_σ orbital is in the plane of the half-occupied Cu $d_{x^2-y^2}$ orbitals with which it has a σ-donor interaction, leading to an intense π^*_σ-to-Cu CT transition. The perpendicular π^*_v orbital has very little overlap with the Cu $d_{x^2-y^2}$ orbitals, producing a weaker LMCT transition at lower energy. For the $[Cu_2(UN-O-)(OOH)]^{2+}$ complex, only one intense π^*-to-Cu CT transition can be identified between 12 000 and 30 000 cm^{-1}. Due to its intensity, it is assigned as the π^*_{Cu}-to-Cu $d_{x^2-y^2}$ transition (π^*_σ will be henceforth labeled π^*_{Cu} in this paper). The second π^* orbital, π^*_H, analogous to the π^*_v orbital of the unprotonated peroxo−Cu complexes, interacts strongly with the proton, leading to significant stabilization of this orbital. Thus, the LMCT transition originating from the π^*_H orbital is expected to be shifted higher in energy than the π^*_v CT transitions in the unprotonated peroxo−Cu complexes. For the $[Cu_2(XYL-O-)(O_2)]^+$ peroxo complex, from which a μ-1,1-hydroperoxo complex is formed by protonation, the π^*_v-to-Cu CT transition is 3900 cm^{-1} lower in energy than the π^*_{Cu}-to-Cu CT transition.[15] For the hydroperoxo complex, the π^*_H-to-Cu CT transition is expected to be at equal or higher energy compared to that of the π^*_{Cu}-to-Cu CT transition. The main source of intensity for the π^*_H-to-Cu LMCT transition is the tilt of the peroxide out of the Cu−O−Cu plane, which mixes π^*_{Cu} and π^*_H orbitals. Mixing of these orbitals also reduces the energy splitting between the two hydroperoxo π^*-to-Cu CT transitions so that only if the π^*_H-to-Cu CT transition is under the 25 200 cm^{-1} band is it expected to have significant intensity.[57]

The RR excitation profiles of the phenolate vibrations in $[Cu_2(UN-O-)(OOH)]^{2+}$ exhibit a maximum around 25 000 cm^{-1}, indicating that some of the absorption intensity in this region is due to phenolate-to-Cu CT. There are two pπ orbitals of phenolate that could give rise to phenolate-to-Cu CT transitions. The correspondence between the absorption intensities of the bands at 30 000 and 21 000 cm^{-1} for the two different complexes in Figure 3 suggests these transitions may be of related origin, i.e., two phenolate-to-Cu CT transitions, although the enhancement of the phenolate vibrations is greater at 25 000 cm^{-1} than it is for excitation near these two bands, indicating an additional phenolate-to-Cu CT transition near 25 000 cm^{-1}.[57] In a study of $[Cu_2(XYL-O-)(OH)]^{2+}$, RR profiles of phenolate vibrations were used to assign a phenolate-to-Cu transition to an unresolved shoulder at 460 nm (21 700 cm^{-1}, $\epsilon \sim 700$ M^{-1} cm^{-1}).[53] Other X-bridged dimers, $[Cu_2(XYL-O-)(X)]$ where X^- is Cl^-, Br^-, or N_3^-, have bands in the 20 000−30 000 cm^{-1} region with intensities of ∼500−2000 M^{-1} cm^{-1} that have been

(53) Ling, J.; Farooq, A.; Karlin, K. D.; Loehr, T. M.; Sanders-Loehr, J. *Inorg. Chem.* **1992**, *31*, 2552−2556.
(54) Pyrz, J. W.; Karlin, K. D.; Sorrell, T. N.; Vogel, G. C.; Que, L., Jr. *Inorg. Chem.* **1984**, *23*, 4581−4584.
(55) Mukherjee, A.; McGlashen, M. L.; Spiro, T. G. *J. Phys. Chem.* **1995**, *99*, 4912−4917.
(56) Pinchas, S. *Spectrochim. Acta* **1972**, *28A*, 801−802.

(57) Each ligand donor orbital can produce two LMCT transitions in a Cu dimer since there are two Cu acceptor orbitals, the symmetric and antisymmetric combinations of the two half-occupied Cu $d_{x^2-y^2}$ orbitals. A transition vector dipole coupling (TDVC) model estimates the intensity ratio of the two components of the π^*_{Cu}-to-Cu CT to be 3:2.[20] Calculations suggest the energy splitting of the two components for this complex is expected to be <3000 cm^{-1} so that the components of the π^*_{Cu}-to-Cu CT transition would not be resolved.

assigned to phenolate-to-Cu CT transitions.[58] The enhancement behavior of the phenolate vibrational modes of $[Cu_2(UN-O-)(OOH)]^{2+}$ is complicated in the sense that they show at least three distinct types of enhancement profiles between 16 000 and 28 000 cm^{-1} and the enhancement behavior varies for different *OPh isotopes (see Supporting Information). This is presumably due to the closely spaced excited states and very mixed phenolate vibrational modes. The important conclusion for the purposes of this study is that there is significant phenolate-to-Cu as well as hydroperoxo-to-Cu CT intensity under the 25 200 cm^{-1} absorption band.

Peroxo−Copper Covalency Estimate from Charge-Transfer Intensity. The integrated absorption intensity of the hydroperoxo-to-Cu CT band at 25 200 cm^{-1} may be used to estimate the magnitude of the donor interaction of peroxide with the copper ions.[17] Since the hydroperoxo-to-Cu CT absorption band overlaps with at least two other CT bands, the integrated absorption intensity attributable to hydroperoxo-to-Cu CT must be approximated. The oscillator strength of Gaussian band 2 in Table 1 (0.13) combined with half the oscillator strength of band 1 (0.03) is considered to provide a rough upper estimate of the hydroperoxo-to-copper CT transition intensity in this complex. The relative peroxo−copper σ donor strength of a series of complexes, given by ratios of the covalencies determined from charge-transfer intensity, shows significant variation and has proven useful for comparison of the bonding in these complexes.[17,20] The ratio of the donor strength of the $[Cu_2(UN-O-)(OOH)]^{2+}$ complex to that of $[Cu_2(UN-O-)(O_2)]^{+}$, the unprotonated complex in which the peroxide is bound only to one copper, is calculated from the peroxo-to-Cu CT intensity to be 1.2. This ratio relates to the amount of metal character in the ligand bonding orbitals and therefore reflects the relative donor strength of the peroxide ligand. The comparable covalencies in the peroxo and hydroperoxo complexes, despite the additional Cu−O bond in the latter, indicates a weak donor interaction with copper in the hydroperoxide complex.

Electronic Structure Calculations. The vibrational data and normal-coordinate analysis show that protonation of $[Cu_2(UN-O-)(O_2)]^{+}$ to form $[Cu_2(UN-O-)(OOH)]^{2+}$ significantly increases the stiffness of the O−O bond. One possible explanation for this effect is an increase in the Cu−O_2 covalency upon protonation. As shown in Figure 2, an additional Cu−O bond is formed in the hydroperoxo−copper complex. This additional Cu−O bonding interaction could shift electron density from peroxide π^* antibonding orbitals to the copper ion, which would strengthen the O−O bond. This explanation for the origin of the strong O−O bond is discounted since analysis of the peroxo- and hydroperoxo-to-Cu CT intensities indicates that there is little increase in the total peroxo−copper covalency, and hence the donor strength, in $[Cu_2(UN-O-)(OOH)]^{2+}$ relative to the unprotonated species. An alternative explanation for the increased O−O bond strength is that protonation of the peroxide directly affects the intra-peroxide bonding so as to increase the stiffness of the O−O bond, independent of changes in the metal-peroxide bonding. To probe the effects of protonation on peroxide O−O bonding, SCF-Xα-scattered wave (SCF-Xα-SW) molecular orbital calculations were performed on simple models of free and copper-bound hydroperoxides.

A. Effect of Protonation on Peroxide. The SCF-Xα-SW MO energy diagram for the HOO^- anion and the hypothetical O_2^{2-} dianion is shown in Figure 6. This diagram uses the orbital labels that will be used in the remainder of this section.[59] Protonation greatly stabilizes the orbitals of the peroxide dianion by decreasing the charge on the dianion to −1. The experimentally determined electron affinity of $HOO^{\bullet}$ is 1.08 eV[60] compared to the −5 eV calculated for the reduction of free superoxide to form the hypothetical O_2^{2-} dianion.[61] Protonation splits the degenerate π^b bonding and π^* antibonding pairs of orbitals of O_2^{2-}. The main O−H bonding interaction is between the H 1s and the peroxide π^b_H orbitals. The π^b_H orbital is shifted to deeper energy than the $\sigma^b(2p_z)$ orbital (Figure 6), and these two orbitals become strongly mixed (Table 4). The other in-plane π^* orbital, π^*_H, is stabilized by about 1 eV relative to $\pi^*_\perp$.

Upon protonation of peroxide, the atomic orbitals of the proton-bound oxygen, O_β, are greatly stabilized relative to those

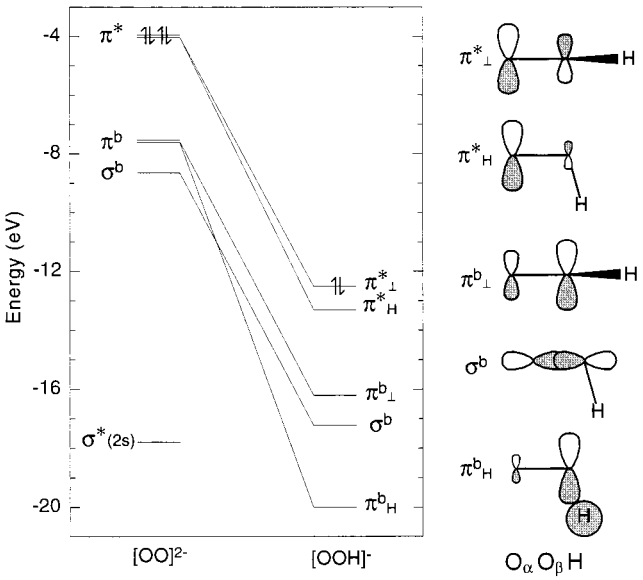

Figure 6. SCF-Xα-SW molecular orbital energy diagram for O_2^{2-} and HOO^- and the molecular orbitals of HOO^-. Electron occupancy is shown for the HOMO orbitals. The MO energies were calculated using a "Watson" sphere of +2 charge surrounding each molecule. (The energies listed for HOO^- in Table 4 are from calculations using a +1 Watson sphere.)

Table 4. Results of SCF-Xα-SW Calculations for the Highest Occupied Valence Two-Electron Orbitals of OOH

orbital label[a]	energy (eV)	% O_α orbitals				% O_β orbitals				%H
		O_α[b]	π_H[c]	σ[c]	$\pi_\perp$[c]	O_β[b]	π_H[c]	σ[c]	$\pi_\perp$[c]	s[d]
$\pi^*_\perp$	−4.73	**67**	0	0	66	**33**	0	0	32	**0**
π^*_H	−5.54	**88**	88	0	0	**8**	6	0	0	**4**
$\pi^b_\perp$	−8.36	**34**	0	0	33	**66**	0	0	65	**0**
$\sigma^b + \pi^b_H$	−9.47	**44**	2	39	0	**56**	9	45	0	**0**
π^b_H + H s	−12.17	**15**	3	8	0	**64**	53	4	0	**21**

[a] Oxygen orbitals are named according to the peroxide parent orbital. [b] Total percentage of orbital partitioned on the peroxo oxygen. [c] $l = 1$ oxygen atom contribution of indicated symmetry with respect to peroxide. [d] Total percentage of orbital partitioned on the peroxide-bound proton.

(58) Karlin, K. D.; Cohen, B. I.; Hayes, J. C.; Farooq, A.; Zubieta, J. *Inorg. Chem.* **1987**, *26*, 147−153.

(59) Subscripts are used to distinguish peroxide π orbitals which are split by bonding with H^+ and/or copper. For the OOH molecule, an H subscript is used to label O_2 π orbitals in the OOH plane and a $\perp$ subscript denotes orbitals with a node in the OOH plane. For the CuOO model, a Cu subscript is used to label the O_2 π orbitals oriented in the CuOO plane and a v subscript indicates the π orbitals with a node in this plane.

(60) Oakes, J. M.; Harding, L. B.; Ellison, G. B. *J. Chem. Phys.* **1985**, *83*, 5400−5406.

(61) Boldyrev, A. I.; Simons, J. *J. Chem. Phys.* **1993**, *98*, 4745−4752.

Table 5. Calculated O−O Bond Lengths (Å)

	r(O−O)		*r*(O−O)
Li(OO)Li	1.61	BeOO	1.68
Li(OOH)	1.54	$[BeOOH]^+$	1.58
$[Li(OOH)Li]^+$	1.53		

on the unprotonated oxygen, O_α. Hence, the π^b and π^* orbitals of peroxide, evenly distributed on O_α and O_β, become strongly polarized in hydroperoxide. As depicted in Figure 6, right, the electron density of both π^b orbitals is more localized on O_β, whereas the electron density of both π^* orbitals is more localized on O_α. Table 4 shows the percentage of each hydroperoxide molecular orbital located on O_α and O_β. The σ^b orbital is not significantly polarized by protonation of peroxide. Hence, protonation has disrupted the O−O π bonding and antibonding interactions, particularly in the OOH plane, while the strong O−O σ-bonding interaction remains.

The SCF-Xα-SW results suggest an increase in O−O bond strength upon protonation since disruption of the O−O π interactions leads to increased O−O bond strength (vide infra). The bond strength cannot be directly calculated using the SCF-Xα-SW calculations since this method does not yield reasonable values for the total energy and thus cannot quantitatively evaluate properties that depend on the molecular potential energy surface, such as the O−O bond length or bond strength.[34,62] Alternatively, ADF density functional LCAO calculations do provide useful values for total energy and are used here to evaluate the change in peroxide O−O bond length with protonation. For these calculations, group 1A and 2A metal ions were added as countercharges for the O_2^{2-} and OOH^- anions. For all models, the optimized geometry places the dioxygen side-on (η^2) to the metal ion whereas the proton binds to only one oxygen with an OOH angle of ∼101°. The calculated equilibrium O−O bond lengths for several $M_xO_2(H)$ species are shown in Table 5. For these peroxo−metal models, the ADF calculations show protonation to cause a decrease in the O−O bond length. This is the case even when an alkali metal ion is removed upon protonation to maintain the same total charge on the molecule.

B. Hydroperoxo−Copper Bonding. SCF-Xα-SW calculations were performed on the $(NH_3)_3CuOOH$ and $(NH_3)_3CuOO$ models shown in Figure 7. These calculations are used to compare copper−hydroperoxide bonding with copper−peroxide bonding and to assess the effects of copper binding on the O−O bond of hydroperoxide. In the crystallographically characterized acylperoxo-bridged analogue of the $[Cu_2(UN{-}O{-})(OOH)]^{2+}$ dimer, the OOAc plane is approximately normal to the N_2CuO_2 equatorial plane of the Cu ions.[25] Therefore, unless otherwise noted, the results below are for the CuOOH *orthog* (Figure 7B) model in which the OOH plane is orthogonal to the N_3CuO plane. To consider the effect of proton placement, calculations were also performed on a second model, labeled CuOOH *planar*, in which the proton is in the N_3CuOO plane (Figure 7C).

In the CuOOH *orthog* model, the main copper−oxygen bonding interaction is between the Cu $d_{x^2-y^2}$ orbital and the π^*_{Cu} (labeled $\pi^*_\perp$ for free hydroperoxide) orbital in the N_3CuO plane (Figure 8, left, middle). The bonding and antibonding interactions between the Cu $d_{x^2-y^2}$ and the π^*_{Cu} orbitals occur in levels 19a and 24a, respectively (Figure 8). This Cu $d_{x^2-y^2}$−π^*_{Cu} interaction is also the principal copper−peroxide bonding interaction in the CuOO model in which the analogous bonding

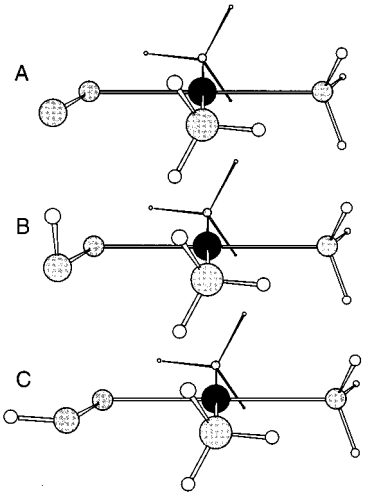

Figure 7. Peroxo− and hydroperoxo−copper structures used for monomer SCF-Xα-SW calculations: (A) CuOO; (B) CuOOH *orthog*; (C) CuOOH *planar*.

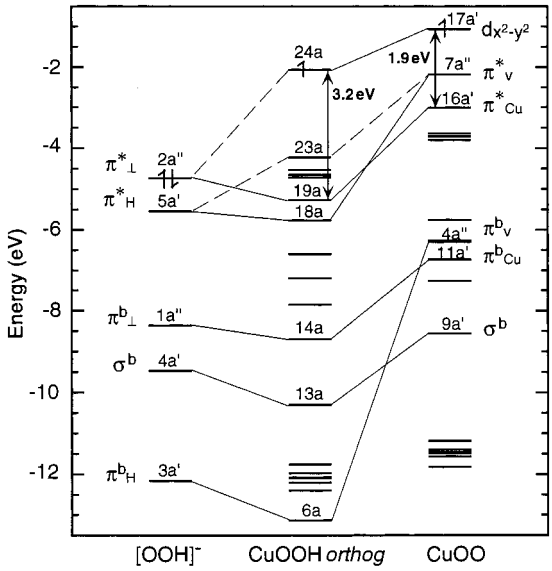

Figure 8. SCF-Xα-SW molecular orbital energy diagram for the HOO^-, CuOOH *orthog*, and CuOO models. Spherical "Watson" countercharges were used for the ionic HOO^- and CuOOH models. Electron occupancy is shown for the HOMO orbitals. The splitting of the π^*_{Cu} and Cu $d_{x^2-y^2}$ orbitals for the protonated and unprotonated complexes is indicated by the arrows.

and antibonding orbitals are 16a′ and 17a′ (Figure 8, right). As determined in the previous section, the $\pi^*_\perp$ orbital in unbound hydroperoxide is stabilized to much deeper binding energy relative to the π^* orbital of O_2^{2-}. Consequently, in the CuOOH *orthog* complex, the π^*_{Cu} orbital (derived from the $\pi^*_\perp$ orbital of free HOO^-) is deeper in energy relative to the Cu $d_{x^2-y^2}$ valence orbital than the π^*_{Cu} orbital in the unprotonated complex (3.2 vs 1.9 eV, Figure 8) with less covalent mixing of the π^*_{Cu} and Cu $d_{x^2-y^2}$ orbitals in the CuOOH complex. Figure 9, top, depicts the HOMO orbital (24a in CuOOH *orthog*, 17a′ in CuOO). Since the HOMO is the antibonding combination of the Cu $d_{x^2-y^2}$ and the π^*_{Cu} orbitals, the peroxide contribution to this orbital is a measure of peroxo−Cu covalency. The hydroperoxide complex exhibits less covalency than the peroxide complex with a 10% hydroperoxide oxygen contribution to the HOMO in CuOOH *orthog* (24a) versus 17% a contribution in CuOO (17a′). In the CuOOH *planar* model, the oxygen contribution to the HOMO is reduced to 7% (Table 6).

(62) Dunlap, B. I.; Connolly, J. W. D.; Sabin, J. R. *J. Chem. Phys.* **1979**, *71*, 3396−3402.

Table 6. Results of SCF-Xα-SW Calculations: $Cu_{x^2-y^2}$ and Peroxo Orbital Comparison

$CuO_\alpha O_\beta$				$O_\alpha O_\beta H$			$CuO_\alpha O_\beta H$ *orthog*				$CuO_\alpha O_\beta H$ *planar*			
orbital	levels	O_α[a]	O_β[a]	orbital	O_α[a]	O_β[a]	orbital	levels	O_α[a]	O_β[a]	orbital	levels	O_α[a]	O_β[a]
$d_{x^2-y^2}$	17a′	12	5				$d_{x^2-y^2}$	24a	8	2	$d_{x^2-y^2}$	17a′	7	0
π^*_v	7, 5a″	42	52	$\pi^*_\perp$	66	32	π^*_{Cu}	19, 24a	34	43	$\pi^*_\perp$	7, 5a″	57	35
$\boldsymbol{\pi^*_{Cu}}$	16, 17a′	**28**	**55**	$\boldsymbol{\pi^*_H}$	**88**	**8**	$\boldsymbol{\pi^*_H}$	18, 23a	**81**	**5**	$\boldsymbol{\pi^*_{H,Cu}}$	14, 17a′	**61**	**6**
π^b_v	4a″	46	42	$\pi^b_\perp$	33	65	π^b_{Cu}	14, 13a	39	30	$\pi^b_\perp$	4a″	34	60
σ^b	9, 11a′	37	41	σ^b	47	49	σ^b	13, 6, 14a	43	43	σ^b	10, 6a′	34	34
$\boldsymbol{\pi^b_{Cu}}$	**11, 9a′**	**38**	**17**	$\boldsymbol{\pi^b_H}$	**5**	**62**	$\boldsymbol{\pi^b_H}$	**6, 13a**	**4**	**53**	$\boldsymbol{\pi^b_{H,Cu}}$	**6, 10a′**	**12**	**50**

[a] Summed oxygen atom $l = 1$ contributions to levels of indicated symmetry with respect to the peroxide unit.

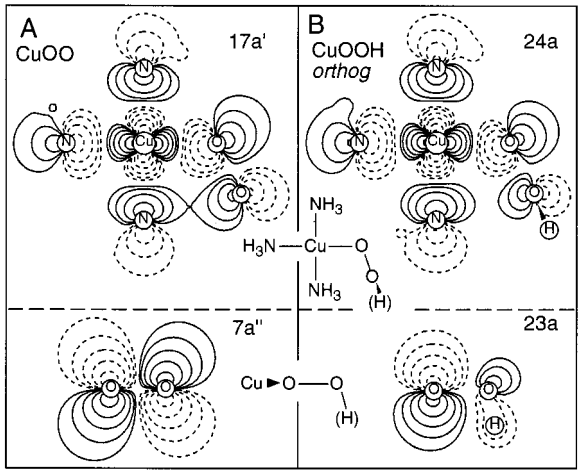

Figure 9. SCF-Xα-SW contour plots of the HOMO (top left, level 17a′) and π^*_v orbitals (bottom left, level 7a″) of the CuOO model and the HOMO (top right, level 24a) and π^*_H (bottom right, level 23a) orbitals of the CuOOH *orthog* model. Contour lines are drawn at ±0.64, ±0.32, ±0.16, ±0.08, ±0.04, and ±0.02 $(e/bohr^3)^{1/2}$.

The SCF-Xα-SW calculations also describe the effects of metal binding on the *intra-peroxide* bonding of the hydroperoxide ligand. The peroxide orbitals are less perturbed by binding of a copper ion than by protonation. Therefore, the peroxide-based orbitals of the $(NH_3)_3CuOOH$ model are very similar to the orbitals of HOO^- described in the previous section and are significantly perturbed relative to the peroxide-based orbitals in the unprotonated complex, $(NH_3)_3CuOO$. Table 6 compares the individual oxygen atom contributions to the peroxide-derived orbitals of CuOO, OOH, CuOOH *orthog*, and CuOOH *planar*. In this table, peroxide orbitals that were split by bonding/antibonding interactions with the Cu are recombined to construct the parent peroxide orbitals. For example the π^*_{Cu} contributions to the 24a and 19a orbitals of CuOOH *orthog* are summed to obtain the π^*_{Cu} orbital.[63] Table 6 shows that the π^*_H orbital in the CuOOH models is localized on O_α, losing its O−O antibonding character and becoming a nonbonding oxygen p orbital (Figure 9, bottom right). Likewise, the π^b_H orbital is localized on O_β and becomes a nonbonding p orbital on O_β. This is in contrast to the CuOO model in which the corresponding π^*_v (Figure 9, bottom left) and π^b_v orbitals have nearly even distributions of electron density on O_α and O_β. In the CuOOH *planar* model, the disruption of the O−O π interactions is distributed between the two π orbital planes differently from the CuOOH *orthog* model, but the combined effect on O−O bonding is approximately the same. In summary, the CuOO model shows a polarization of the peroxide π orbitals upon protonation similar to that of the unbound O_2^{2-} model.

Discussion

Significant changes in bonding occur when the peroxo−copper complex, $[Cu_2(UN{-}O{-})(O_2)]^+$, is protonated to form the μ-1,1-hydroperoxo-bridged complex, $[Cu_2(UN{-}O{-})(OOH)]^{2+}$. The frequency of the O−O stretch increases from 803 to 892 cm^{-1}, and the peroxo π^*_{Cu}-to-Cu CT transition energy increases from 19 900 to 25 200 cm^{-1}. The 892 cm^{-1} ν(O−O) of the $[Cu_2(UN{-}O{-})(OOH)]^{2+}$ complex is higher than the ν(O−O) observed for any peroxo−copper complex. The lower hydroperoxo π^*_{Cu}-to-Cu CT intensity per copper shows this complex to have a relatively weak σ-donor interaction with the copper ions compared to those of other peroxo−copper(II) complexes. For peroxo−metal complexes, the intra-peroxide bond strength is normally correlated to the degree of σ-donation from the antibonding π^* peroxo orbitals to the metal.[17] Since the μ-1,1-hydroperoxo-bridged complex exhibits relatively weak σ donation to the copper ions, the direct effect of protonation on intra-peroxide bonding, not changes in the peroxo−copper donor interaction, must be responsible for the high ν(O−O).

Density functional calculations were performed to determine the effect of protonation on unbound peroxide. The molecular orbital diagram in Figure 6 demonstrates the effects of protonation on intra-peroxide bonding. The proton stabilizes the atomic orbitals on O_β (the proton-bound atom) relative to O_α. Thus the peroxide π^b orbitals become localized on O_β and the corresponding peroxide π^* orbitals become localized on O_α. This polarization is most dramatic for the peroxide π orbitals in the OOH plane. The π^b_H orbital participates in a bonding interaction with the proton, and the resulting polarization of this orbital results in what is essentially an O−H σ-bonding orbital with very little interaction with the other O atom. Conversely, the π^*_H orbital becomes essentially an O_α p orbital showing little interaction with the other O atom. Thus both the π-bonding and the π-antibonding interactions are disrupted by protonation, particularly in the OOH plane. The net effect of filled bonding and antibonding sets of orbitals is weakly repulsive, so removing these O−O π interactions strengthens the O−O bond.[64] It is important to note that the $\sigma^b(2p_z)$ orbital, which makes the greatest contribution to O−O bonding in both peroxide and hydroperoxide, is only slightly disrupted upon protonation since the p_z orbital of the proton-bound oxygen is nearly perpendicular to the O−H bond.

This molecular orbital description of the effect of protonation on O−O bonding can also be stated in terms of valence shell electron pair repulsion theory (VSEPR). Protonation of O_2^{2-} changes one oxygen lone pair to an O−H bonding electron pair, decreasing the O−O lone-pair-lone-pair repulsion and strength-

(63) Some of the peroxide orbitals that are recombined have different distributions of partitioned charge with respect to the two oxygen atoms so that the recombined orbitals imply a degree of O−O electron density localization different from that observed in the original individual orbitals. This difference is small and does not significantly affect the results.

(64) Murrell, J. N.; Kettle, S. F. A.; Tedder, J. M. *The Chemical Bond*, 2nd ed.; John Wiley & Sons: Chichester, U.K., 1985.

Table 7. Relative Covalencies and Vibrational Frequencies of (Hydro)peroxo−copper(II) Complexes[a]

		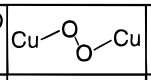	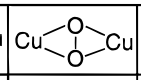	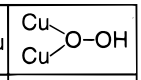
α^2 (f)	1 (0.14)	1.9 (0.27)	3.7 (0.50)	1.2 (0.16)
$\nu_{O\text{-}O}$ (k)	803 (2.9)	832 (3.1)	763 (2.4)	889 (3.7)
$\nu_{Cu\text{-}O}$ (k)	488 (1.8)	561 (1.9)	572 (1.4)	505/322 (1.2)

[a] α^2 is the relative peroxide ligand covalency, f is the oscillator strength, ν is the vibrational frequency in units of cm^{-1}, and k is the Urey−Bradley force constant in mdyn/Å.

ening the O−O bond. This VSEPR argument has been invoked to explain the increasing O−O stretching frequency for the series OOH^-, HOOH, H_2OOH^+.[27]

Further SCF-Xα-SW calculations were performed on $(NH_3)_3$-CuOO and $(NH_3)_3$CuOOH models to determine the effect of Cu binding on the hydroperoxide bonding picture presented above and to determine the effect of protonation on Cu−O bonding. The resulting CuOOH bonding description accounts for the experimentally observed increase in the stiffness of the O−O bond upon protonation of the $[Cu_2(UN{-}O{-})(OOH)]^{2+}$ complex as well as the decrease in the Cu−O covalency per Cu−O bond. First, protonation of the CuOO model causes a similar polarization of the $\pi^b{}_H$ and $\pi^*{}_H$ orbitals observed for free peroxide and the $\sigma^b(2p_z)$ orbital remains unaffected. Thus, the same explanation for the stiffening of the O−O bond upon protonation of free peroxide applies to the bound peroxide as well. Second, protonation greatly stabilizes the peroxide orbitals, increasing electron affinity and also making hydroperoxide a more innocent (less covalent) ligand than peroxide. This is reflected in the calculated decrease in covalency for the CuOOH monomer model (10%) relative to the CuOO model (17%; see Figure 9, top, and Table 6) and the decrease in covalency per Cu−O bond in the $[Cu_2(UN{-}O{-})(OOH)]^{2+}$ complex. The decrease in peroxo−copper covalency shown in these SCF-Xα-SW calculations is consistent with the decrease in covalency per Cu−O bond derived from the experimental peroxo-to-Cu CT absorption intensity (∼1:0.6; Table 7).

The description of hydroperoxo−copper bonding presented above predicts that protonation will generally increase peroxide O−O bond strength. This appears to be the case for several examples in which direct comparison can be made between the unprotonated and protonated forms of the same peroxo species. Raman studies by Eysel and Thym on alkali metal peroxide salts and their corresponding protonated MOOH salts show an increase in ν(O−O) of ∼90 cm^{-1}, from 740−790 cm^{-1} for the peroxides to 840−880 cm^{-1} for the hydroperoxides.[65] This observation is consistent with our ADF calculations on simple alkali metal and alkaline earth metal peroxides and hydroperoxides which show shortening of the O−O bond with protonation. Christie et al.[27] noted the increase in ν(O−O) upon successive protonation of peroxide: O_2^{2-} (750 cm^{-1}),[65] HOO^- (836 cm^{-1}),[66,67] H_2O_2 (864−881 cm^{-1}),[50,51,68] and $H_3O_2^+$ (875 cm^{-1}).[27] Crystal structures of the μ-1,2-peroxo-bridged cobalt dimer $[(en)_2Co(NH_2,O_2)Co(en)_2]^{3+}$ and the corresponding protonated complex, a μ-1,1-hydroperoxo-bridged dimer, $[(en)_2Co(NH_2,OOH)Co(en)_2]^{4+}$, show a decrease in the O−O bond length from 1.46 to 1.42 Å.[26,69,70] The Herschbach−Laurie empirical relationship between bond length and force constant predicts that a decrease of 0.04 Å should give an increase in ν(O−O) of ∼40 cm^{-1}.[71] Despite these examples in which protonation increases ν(O−O) *in the same complex*, transition metal−hydroperoxo complexes do not collectively have higher ν(O−O) values than peroxo−metal complexes. All other factors being equal, protonation should increase ν(O−O). However, the metal d^n configuration and the charge donor properties of the other ligands will also affect the observed ν(O−O). For example, the ν(O−O) values for cis μ-1,2-peroxo−Fe(III) complexes are generally high. The one known hydroperoxo−Fe(III) complex, oxyhemerythrin, has a ν(O−O) of 844 cm^{-1}.[72] The d^5 configuration of Fe(III) allows an additional peroxide donor interaction with the metal.[73] Also, oxyhemerythrin has an extremely strong donor ligand, a bridging oxo group. The one-hole d^9 configuration of copper permits only one peroxide donor interaction, revealing the intrinsic increase in ν(O−O) upon protonation.

The bonding in the μ-1,1-hydroperoxo−copper complex may be compared with the previously studied series of peroxo−copper complexes. Table 7 compares the Cu−O covalency, ν(O−O), and ν(Cu−O) for end-on monomer,[74] end-on trans μ-1,2 dimer, and side-on dimer peroxo−copper complexes and the for μ-1,1-hydroperoxo-bridged dimer. The three peroxo−copper complexes have one, two, and four Cu−O bonds, respectively. The peroxo donor strengths in these complexes, as determined by peroxo-to-Cu CT intensity, have a ratio of 1:1.9:3.7.[17,20] Thus, all three peroxo−copper complexes have roughly the same covalency per Cu−O bond. Compared to the peroxo-Cu complexes, the hydroperoxo−copper complex has about two-thirds as much σ donation per Cu−O bond. This diminished donor interaction is a consequence of the large stabilization of the peroxide π^* orbitals relative to the Cu $d_{x^2-y^2}$ orbital upon protonation, as shown by the SCF-Xα-SW calculations.

The O−O stretching frequency in peroxo−copper complexes does not follow such a clear trend with respect to the number of Cu−O bonds.[17,20] In general, the O−O stretching frequency of peroxo−copper complexes is expected to be greater for more covalent complexes due to charge donation out of the π^*-antibonding peroxide orbitals. This is the case for the monomer and trans end-on dimer complexes. The more covalent end-on dimer has an O−O stretching frequency of 832 cm^{-1}, compared to 803 cm^{-1} in the monomer. The side-on complex does not fit this expected relationship between peroxo−copper covalency and O−O stretching frequency. The peroxo−copper covalency is very high in the side-on dimer, but the O−O stretch of 740 cm^{-1} is the lowest observed in any peroxo−metal complex. This

(65) Eysel, H. H.; Thym, S. *Z. Anorg. Allg. Chem.* **1975**, *411*, 97−102.
(66) Giguère, P. A.; Knop, O. *Can. J. Chem.* **1959**, *37*, 1794.
(67) Vasquez, G. J.; Buenker, R. J.; Peyerimhoff, S. D. *Chem. Phys.* **1989**, *129*, 405−415.
(68) Huang, H. H.; Xie, Y.; Schaefer, H. F. *J. Phys. Chem.* **1996**, *100*, 6076−6080.
(69) Thewalt, U. *Z. Naturforsch.* **1970**, *25B*, 569−571.
(70) This comparison should be considered tentative since there is disorder in the μ-1,1 structure which primarily affects the Co_2O_2 unit. The *R* values for the μ-1,1- and μ-1,2-hydroperoxo−cobalt structures are 0.075 and 0.076, respectively. Error estimates for r(O−O) are not given. Raman experiments on the similar octaammine complex $[(NH_3)_4Co(O_2,NH_2)Co(NH_3)_4]^{3+}$ in aqueous solution show little if any increase in frequency upon protonation.
(71) Herschbach, D. R.; Laurie, V. W. *J. Chem. Phys.* **1961**, *35*, 458−463.
(72) Shiemke, A. K.; Loehr, T. M.; Sanders-Loehr, J. *J. Am. Chem. Soc.* **1986**, *108*, 2437−2443.
(73) Brunold, T. C.; Tamura, N.; Kitajima, N.; Moro-oka, Y.; Solomon, E. I. *J. Am. Chem. Soc.*, in press.
(74) Although the "end-on monomer" peroxo−copper complex contains two copper ions, the term "monomer" is used since the peroxide has been shown to bind to only one of these copper ions (Figure 2, left).

is attributed to an additional peroxo−copper interaction particular to the side-on bridged structure, in which the peroxide σ^* orbital acts as a π acceptor, weakening the O−O bond.[19] In contrast to the side-on dimer, the μ-1,1-hydroperoxide complex has a very high 889 cm^{-1} ν(O−O) but a relatively low peroxo−copper covalency. In this case, it is the bonding with the proton that accounts for this deviation from the positive correlation between Cu−O covalency and ν(O−O).

It is difficult to use the Cu−O frequencies to estimate relative Cu−O bond strengths since the Cu−O internal coordinate is normally much more mixed with other internal coordinates than the O−O stretch and this mixing is not accurately accounted for in the very simplified normal-coordinate analyses. Also, in dimers there are symmetric and antisymmetric combinations of the Cu−O stretches, of which often only one is observed. However, it is worth noting that the Cu−O force constants generally reflect the relative Cu−O strengths expected from the covalency estimates. The μ-1,1-hydroperoxide complex has a lower Cu−O covalency per Cu−O bond than the peroxo−copper complexes and also has the lowest Cu−O force constant. Comparing the frequencies directly, the average of the ν_s(Cu−O) and ν_{as}(Cu−O) frequencies for the μ-1,1-hydroperoxo-bridged dimer is 75 cm^{-1} lower than the Cu−O frequency of the unprotonated monomer complex.

On the basis of their electronic structure descriptions, both the side-on dimer and the μ-1,1-hydroperoxide dimer are expected to be more electrophilic than the end-on monomer and dimer. In the μ-η^2:η^2 side-on dimer, the electrophilicity of the peroxide is due to strong σ donation to copper, while, in the μ-1,1-hydroperoxide dimer, it is due to strong charge donation to the proton. Experiments show that the hydroperoxo and side-on complexes are reactive for oxo transfer to readily oxidizable nucleophilic substrates such as PPh_3 and tetrahydrothiophene.[22,75] In addition, one side-on peroxo complex is able to perform intramolecular oxygenation of the aryl ring of its dinucleating ligand.[1,76] In contrast, the end-on monomer and dimer are not reactive for oxo transfer. The side-on peroxo dimers are also capable of one-electron oxidative coupling of phenols, presumably via hydrogen atom abstraction. The more negatively charged peroxides of the end-on monomer and trans dimer cannot perform this oxidation reaction.[75] The μ-1,1-hydroperoxo dimer, despite its electrophilicity, is also unable to perform this oxidative coupling.[22] This may be due to the high strength of the O−O bond, which must be broken in this reaction. We suggest that, due to the high O−O bond strength, hydroperoxide complexes are not activated for one-electron oxidations but that two-electron oxo-transfer reactions provide sufficient driving force to break the O−O bond.

The enzyme laccase uses four copper ions to catalyze the four-electron reduction of dioxygen to water.[5] Three of these coppers form a trinuclear copper site,[77,78] and the fourth is a blue copper electron-transfer site ~12 Å away. In the T1Hg derivative of laccase, the blue copper has been replaced by Hg[79] and the fully ($3e^-$) reduced protein reacts with oxygen to form a quasi-stable intermediate in which dioxygen has been reduced by two electrons to the peroxide level and the copper oxidation states are I, II, and II.[7] Spectroscopic studies have led to the proposal of two alternative models for this intermediate.[8] In one, peroxide is bound to all three copper ions of the trinuclear site in a μ_3-$(\eta^1)_3$ fashion. In the second model, a hydroperoxide bridges the Cu(I) and one of the Cu(II) ions in a μ-1,1 fashion. The electronic structure of μ-1,1-bridging hydroperoxide may promote further reduction to water in several ways. First, protonation greatly stabilizes the peroxide π^* orbitals, making the binding and reduction of dioxygen to peroxide less reversible. Second, protonation increases the electron affinity of peroxide and activates it for further reduction by a large stabilization of the peroxide orbitals (Figure 6), including the empty peroxide σ^* orbital. Third, the strong O−O bond may favor the two-electron reduction of the hydroperoxide and prevent one-electron oxidation reactions due to the large driving force required to break the O−O bond. This could avoid the hydrogen abstraction chemistry observed for the side-on species (vida supra) and the resulting radical species. In the alternative μ_3-$(\eta^1)_3$ model for the intermediate, peroxide binding to two Cu(II) and a Cu(I) ion would also be expected to yield a strong intra-peroxide O−O bond, in this case due to charge donation out of the peroxide π^* orbitals. This covalent interaction would also make the peroxide more electronegative and prone to further reduction.

In summary, this work presents a spectroscopic and electronic structural study of a hydroperoxo−copper model complex. Protonation of the $[Cu_2(UN-O-)(O_2)]^+$ peroxo−copper complex to yield this μ-1,1-hydroperoxo-bridged complex increases the frequency of the O−O stretch, raises the peroxide-to-Cu CT transition energy, and decreases peroxo−Cu covalency. Calculations relate these changes to the effect of protonation on intra-peroxide bonding and orbital energies. A strong O−O bond and high peroxide electron affinity are expected to be general features of hydroperoxo−metal complexes and to make important contributions to their reactivity.

Acknowledgment. The authors are grateful to Drs. M. Abe (Hokkaido University, Japan) and N. N. Murthy (IIT, Madras, India) for their time and effort in preparing the complexes used in this study. This work was supported by grants from the National Institutes of Health (DK31450 to E.I.S. and GM28962 to K.D.K.).

Supporting Information Available: Listings of Cartesian coordinates, input parameters, and results for SCF-Xα-SW calculations and Cartesian coordinates for the normal-coordinate analysis and a figure showing the Raman spectra of $[Cu_2(UN-O-)(OOH)]^{2+}$ with 407 and 458 nm excitation (5 pages). Ordering information is given on any current masthead page.

IC980606C

(75) Paul, P. P.; Tyeklár, Z.; Jacobson, R. R.; Karlin, K. D. *J. Am. Chem. Soc.* **1991**, *113*, 5322−5332.
(76) Karlin, K. D.; Hayes, J. C.; Gultneh, Y.; Cruse, R. W.; McKown, J. W.; Hutchinson, J. P.; Zubieta, J. *J. Am. Chem. Soc.* **1984**, *106*, 2121−2128.
(77) Allendorf, M. D.; Spira, D. J.; Solomon, E. I. *Proc. Natl. Acad. Sci. U.S.A.* **1985**, *82*, 3063−3067.
(78) Spira-Solomon, D. J.; Allendorf, M. D.; Solomon, E. I. *J. Am. Chem. Soc.* **1986**, *108*, 5318−5328.
(79) Morie-Bebel, M. M.; Morris, M. C.; Menzie, J. L.; McMillin, D. R. *J. Am. Chem. Soc.* **1984**, *106*, 3677−3678.